

# Pion and Kaon Polarizabilities and Radiative Transitions

Murray A. Moinester and Victor Steiner

School of Physics and Astronomy, R. and B. Sackler Faculty of Exact Sciences,  
Tel Aviv University, 69978 Ramat Aviv, Israel,  
e-mail: murraym@silly.tau.ac.il, steiner@gluon.tau.ac.il

**Abstract.** CERN COMPASS plans measurements of  $\gamma\pi$  and  $\gamma K$  interactions using 50-280 GeV pion (kaon) beams and a virtual photon target. Pion (kaon) polarizabilities and radiative transitions will be measured via Primakoff effect reactions such as  $\pi^-\gamma \rightarrow \pi^-\gamma$  and  $\pi^-\gamma \rightarrow \text{meson}$ . The former can test a precise prediction of chiral symmetry; the latter for  $\pi\gamma \rightarrow a_1(1260)$  is important for understanding the polarizability. The radiative transition of a pion to a low mass two-pion system,  $\pi^-\gamma \rightarrow \pi^-\pi^0$ , can also be studied to measure the chiral anomaly amplitude  $F_{3\pi}$  (characterizing  $\gamma \rightarrow 3\pi$ ) arising from the effective Chiral Lagrangian. We review here the motivation for the above physics program. We describe the beam, target, detector, and trigger requirements for these experiments. We also describe FNAL SELEX attempts to study related physics via the interaction of 600 GeV pions with target electrons. Data analysis in progress aims to identify the reactions  $\pi e \rightarrow \pi'e'\pi^0$  related to the chiral anomaly, and  $\pi e \rightarrow \pi'e'\gamma$  related to pion polarizabilities.

## 1 Introduction

Pion and kaon polarizabilities and associated radiative transitions may be measured in the CERN COMPASS experiment (Bradamante, Paul et al. [1996], Moinester [1994]). Hadron ( $h$ ) radiative transitions may be measured by the Coulomb coherent production reactions  $\gamma h \rightarrow h^*$ , for pions and kaons. The cross sections of these reactions are proportional to the radiative widths  $\Gamma(h^* \rightarrow h\gamma)$ . The polarizabilities are obtained from precision measurements of the  $\gamma h \rightarrow \gamma h$   $\gamma$ -hadron Compton scattering. For the pion and kaon, chiral perturbation theory ( $\chi$ PT) leads to precision predictions for the polarizabilities (Holstein [1990], Babusci et al. [1992]). Precision measurements of polarizabilities therefore subject the  $\chi$ PT techniques of QCD to new and serious tests.

### 1.1 Pion Polarizabilities via Primakoff Scattering

For the pion polarizability,  $\gamma\pi$  scattering was measured (with large uncertainties) with 40 GeV pions (Antipov et al. [1983]) via radiative pion scattering (pion Bremsstrahlung) in the nuclear Coulomb field:

$$\pi + Z \rightarrow \pi' + \gamma + Z'. \quad (1)$$

In this measurement, the incident pion Compton scatters from a virtual photon in the Coulomb field of a nucleus of atomic number  $Z$ ; and the final state  $\gamma$  and pion are detected in coincidence. The radiative pion scattering reaction is equivalent to  $\gamma + \pi^- \rightarrow \gamma + \pi^-$  scattering for laboratory  $\gamma$ 's of order 1 GeV incident on a target  $\pi^-$  at rest. It is an example of the well tested Primakoff formalism (Jensen et al. [1983], Zielinski et al. [1984]) that relates processes involving real photon interactions to production cross sections involving the exchange of virtual photons.

In the 40 GeV radiative pion scattering experiments, it was shown experimentally (Antipov et al. [1983]) and theoretically (Galperin et al. [1980]) that the Coulomb amplitude clearly dominates, and yields sharp peaks in  $t$ -distributions at very small squared four momentum transfers ( $t$ ) to the target nucleus  $t \leq 6 \times 10^{-4}(\text{GeV}/c)^2$ . Backgrounds from strong processes were low. The backgrounds are expected to be lower at the higher energy (280 GeV) planned for the CERN COMPASS experiment.

**All polarizabilities in this paper are expressed in Gaussian units of  $10^{-43} \text{ cm}^3$ .** The  $\chi$ PT prediction (Holstein [1990]) for the pion polarizability is  $\bar{\alpha}_\pi = 2.7$ . Holstein [1990] showed that meson exchange via a pole diagram involving the  $a_1(1260)$  resonance provides the main contribution ( $\bar{\alpha}_\pi = 2.6$ ) to the polarizability. Xiong et al. [1992] assuming  $a_1$  dominance find  $\bar{\alpha}_\pi = 1.8$ . For the kaon, the  $\chi$ PT polarizability prediction (Holstein [1990]) is  $\bar{\alpha}_\pi = 0.5$ . A more extensive theoretical study of kaon polarizabilities was given recently (Ebert and Volkov [1996]).

## 1.2 Pion Polarizabilities via Inelastic $\pi e$ Scattering

Pion-electron elastic scattering  $\pi e \rightarrow \pi' e'$  has been studied in SELEX (Russ et al. [1995]) at Fermilab with 600 GeV energy pion beams and electron targets (atomic electrons in nuclear targets) to measure the low momentum part of the pion form factor, and thereby the charge radius of the pion. Sigma-electron scattering was also studied. These reactions were studied via a trigger that required two negative charged particles in the final state, both over 25 GeV. Various methods of particle identification are utilized to assure that one of the final state particles is an electron. The electron signature together with energy/momentum balance assure that the incident hadron interacts with an electron, and not with the target nucleus.

With the same trigger, one may also study the virtual Compton scattering (VCS) process  $\pi e \rightarrow \pi' e' \gamma$  related to the generalized pion polarizabilities  $\bar{\alpha}_\pi(k)$  and  $\bar{\beta}_\pi(k)$ , which depend on momentum transfer ( $k$ ) to the electron (Drechsel et al. [1997], Guichon et al. [1995]). In the limit of zero momentum transfer, these reduce to the usual Compton polarizabilities. For the VCS reaction, the Bethe-Heitler (BH) amplitude ( $\gamma$  from initial or final state electron, not from the pion Compton amplitude) dominates over the Compton amplitude. For VCS on the pion, the Compton amplitude should be relatively more enhanced compared to

BH for events in which the angle between  $\gamma$  and electron is large. The VCS process and planned VCS experiments (for the proton) at electron accelerators have been discussed extensively in the present workshop. Theoretical calculations and simulations are in progress (Drechsel et al. [1997]) for pion VCS to understand the sensitivity to the generalized polarizabilities for this reaction. Data from SELEX are being analyzed for pion VCS. It is not clear at this stage of the analysis whether or not the signal to background in SELEX will be sufficiently good to get quality data for the VCS process.

### 1.3 Radiative Transitions via Primakoff and Inelastic Electron Scattering

In addition to polarizability measurements, COMPASS may also study radiative transitions of incident mesons to higher excited states. COMPASS may obtain new data (Moinester et al. [1997]) for radiative transitions leading from the pion to the  $\rho$ ,  $a_1(1260)$ , and  $a_2(1320)$ ; and for the kaon to  $K^*$ . Searches for exotic mesons (hybrids) are also possible in this way (Moinester et al. [1997]). The  $\rho$  data is obtained with a  $\gamma\pi$  trigger, while most of the others require a particle multiplicity trigger. Radiative transition widths are predicted by vector dominance and quark models. Independent and higher precision data for these and higher resonances would be valuable in order to allow a more meaningful comparison with theoretical predictions. For example, the  $\rho \rightarrow \pi\gamma$  width measurements (Jensen et al. [1983]) range from 60 to 81 keV; and the  $a_1(1260) \rightarrow \pi\gamma$  width measurement (Zielinski et al. [1984]) is  $0.64 \pm 0.25$  MeV. FNAL SELEX data are being analyzed now to identify the  $\pi e \rightarrow \rho e'$  inelastic electron scattering reaction. Clean data for this reaction would allow a determination of the  $\rho \rightarrow \pi\gamma$  radiative width from a measure of the transition form factor (near zero momentum transfer).

### 1.4 Chiral Anomaly

Another interesting meson radiative transition involves the chiral anomaly term of the effective Chiral Lagrangian. COMPASS may study the Chiral Axial Anomaly with 50-280 GeV pion beams with the same  $\gamma\pi$  trigger as needed for polarizability. The abnormal intrinsic parity (chiral anomaly) component of the effective Chiral Lagrangian predicts (Holstein [1996], Moinester [1995])  $F_{3\pi} = 9.7 \text{ GeV}^{-3}$ ,  $O(p^4)$ , for the  $\gamma \rightarrow 3\pi$   $F_{3\pi}$  amplitude at threshold.  $F_{3\pi}$  was measured (Antipov et al. [1983]) with 40 GeV pions. They studied pion production by a pion in the nuclear Coulomb field near threshold via the Primakoff reaction:

$$\pi^- + Z \rightarrow \pi^{-'} + \pi^0 + Z'. \quad (2)$$

This reaction is equivalent to  $\pi^- + \gamma \rightarrow \pi^{-'} + \pi^0$ , a radiative transition to a low mass two-pion system. The cross section for this Primakoff reaction is proportional to  $F_{3\pi}^2$ . Low- $t$  events were selected in the analysis in order to isolate the

Primakoff process. Diffractive production of the two pion final state via Pomeron exchange is blocked by G-parity conservation. The low statistics ( $\sim 200$ ) experiment (Antipov et al. [1983]) reported  $F_{3\pi}=12.9 \pm 0.9(\text{stat})\pm 0.5(\text{sys}) \text{ GeV}^{-3}$ , which differs from the  $O(p^4)$  expectation. More precise data are needed for this amplitude. The expected number of near threshold two-pion events in COMPASS is several orders of magnitude larger than in all previous experiments (Moinester [1995]).

With a 600 GeV pion beam and a target electron, one may also study  $e\pi \rightarrow e'\pi'\pi^0$  events, where the two  $\gamma$ 's detected in the  $\gamma$  calorimeter have a  $\pi^0$  invariant mass, and the  $\pi\pi^0$  system has invariant mass lower than the  $\rho$ . Such inelastic data provides a means complementary to the Primakoff scattering to determine the chiral anomaly transition form factor (Holstein [1996]) and amplitude  $F_{3\pi}$ . Analysis of SELEX data in search of this reaction is in progress.

## 2 Pion Polarizabilities

For the  $\gamma\pi$  interaction at low energy,  $\chi$ PT provides a rigorous way to make predictions via a Chiral Lagrangian written in terms of renormalized coupling constants  $L_i^r$  (Gasser and Leutwyler [1985]). With a perturbative expansion of the effective Lagrangian, the method establishes relationships between different processes in terms of the  $L_i^r$ . For example, the radiative pion beta decay and electric pion polarizability are expressed as (Holstein [1990]):

$$F_A/F_V = 32\pi^2(L_9^r + L_{10}^r); \quad \bar{\alpha}_\pi = \frac{4\alpha_f}{m_\pi F_\pi^2}(L_9^r + L_{10}^r); \quad (3)$$

where  $F_\pi$  is the pion decay constant,  $F_A$  and  $F_V$  are the axial vector and vector coupling constants in the decay, and  $\alpha_f$  is the fine structure constant. The experimental ratio  $F_A/F_V = 0.45 \pm 0.06$ , leads to  $\bar{\alpha}_\pi = -\bar{\beta}_\pi = 2.7 \pm 0.4$ , where the error shown is due to the uncertainty in the  $F_A/F_V$  measurement (Holstein [1990], Babusci et al. [1992]).

The pion polarizabilities deduced by Antipov et al. [1983] in their low statistics experiment ( $\sim 7000$  events) were  $\bar{\alpha}_\pi = -\bar{\beta}_\pi = 6.8 \pm 1.4 \pm 1.2$ . It was assumed in the analysis that  $\bar{\alpha}_\pi + \bar{\beta}_\pi = 0$ , as expected theoretically (Holstein [1990]). The deduced polarizability value, not counting the large error bars, is some three times larger than the  $\chi$ PT prediction. **The available polarizability results have large uncertainties. There is a clear need for new and improved radiative pion scattering data.**

## 3 Experimental Requirements

We considered the beam, detector, and trigger requirements for polarizability, chiral anomaly, and hybrid meson studies in the CERN COMPASS experiment (Moinester et al. [1997]). We begin for illustration with pion polarizability measurements via the reaction  $\pi^- + Z \rightarrow \pi^{-'} + \gamma + Z'$  with a 300 GeV pion beam.

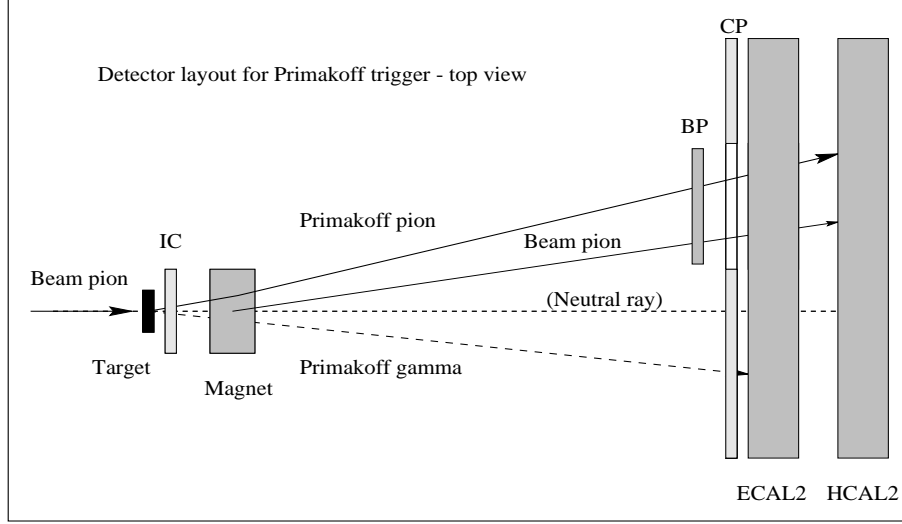


**Fig. 1.** Detector layout for Primakoff trigger.

The beam energy is chosen to be maximal, since that pushes the energy spectrum of final state  $\gamma$ 's and  $\pi^0$ 's to be highest, and thereby the detection acceptance for  $\pi^0$ 's for a given size ECAL2 electromagnetic calorimeter will be maximal. Higher beam energy also gives a higher acceptance for Primakoff production of high mass mesons. Fig. 1 shows the detector layout for this experiment. Proceeding downstream, we consider the scintillation detectors IC (Interaction Counter), BP (Beam/Primakoff fiducial detector), CP (Charged Particle), and the  $\gamma$ /hadron calorimeters ECAL2/HCAL2. The function of these detectors in the trigger will be described below.

### 3.1 Monte Carlo Simulations

We carried out Monte Carlo simulations with the code POLARIS, an event generator for polarizability studies; and ANOMALY, for chiral anomaly studies (Steiner et al. [1995]). In this report, we show only the POLARIS results. POLARIS produces events of the type Eq. 1, based on the theoretical Primakoff  $\gamma\pi$  Compton scattering cross section. The four-momentum of each particle is  $p_1, p_2, p_1', p_2', k, k'$ , respectively, as shown in Fig. 2. In the one-photon exchange domain, this reaction is equivalent to  $\gamma + \pi \rightarrow \gamma' + \pi'$ , and the four-momentum of the incident virtual photon is  $k = p_2 - p_2'$ . We have therefore  $t = k^2$  with  $t$  the square of the four-momentum transfer to the nucleus,  $F(t)$  the nuclear form factor (essentially unity at small  $t$ ,  $\sqrt{s}$  the mass of the  $\gamma\pi$  final state, and  $t_0$  the minimum value of  $t$  to produce a mass  $\sqrt{s}$ . The momentum modulus  $|\mathbf{k}|$  (essentially equal to  $p_T$ ) of the virtual photon is in the transverse direction, and is equal and opposite to the momentum  $p_T$  transferred to the target nucleus. For

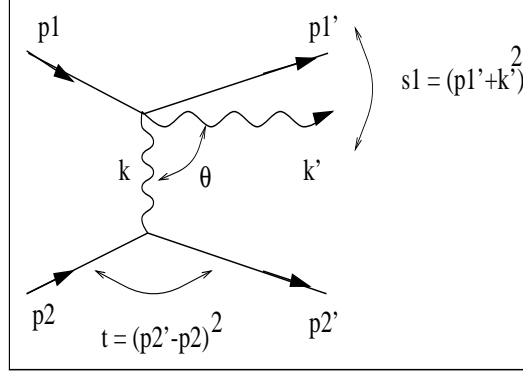


**Fig. 2.** The Primakoff  $\gamma$ -hadron Compton process and kinematic variables (4-momenta):  $p1, p1'$  = for initial/final hadron,  $p2, p2'$  = for initial/final target,  $k, k'$  = for initial/final gamma, and  $\theta$  the scattering angle of the  $\gamma$  in the alab frame.

the generated events, the pion and  $\gamma$  laboratory variables may be given gaussian spreads to simulate measurement errors, and acceptance cuts may be used (optional). Finally, the simulated events are taken to be these "measured" values. The pion polarizability is extracted via a fit of the theoretical cross section to the scattered  $\gamma$  angular distribution in the projectile (alab) rest frame. The total Primakoff cross section is computed by integrating numerically the differential cross section  $\sigma(s, t, \theta)$  of Eq. 4 below for the Primakoff Compton process.

The code ANOMALY produces events with the topology of Eq. 2, following the techniques of POLARIS.

### 3.2 Primakoff $\gamma\pi$ Compton Event Generator

We describe the event generator for the radiative scattering of the pion in the Coulomb field of a nucleus (Steiner et al. [1995]). In the pion alab frame, the nuclear Coulomb field effectively provides a virtual photon beam incident on a pion target at rest. We have for the variable  $t = k^2 \equiv M^2$ , where  $k$  is the 4-momentum transferred to the nucleus, and  $M$  is the virtual photon mass. Since  $t = 2M_Z[M_Z - E(Z', lab)] < 0$ , the virtual photon mass is imaginary. To approximate real pion Compton scattering, the virtual photon should be taken to be almost real. For small  $t$ , the electromagnetic contribution to the scattering amplitude is large compared to meson and Pomeron exchange contributions.

The Primakoff differential cross section of the process of Eq. 1 in the alab frame may be expressed as (Starkov [1982]):

$$\frac{d^3\sigma}{dt d\omega d\cos\theta} = \frac{\alpha_f Z^2}{\pi\omega} \cdot \frac{t - t_0}{t^2} \cdot \frac{d\sigma_{\gamma\pi}(\omega, \theta)}{d\cos\theta}, \quad (4)$$

where the  $\gamma\pi$  cross section is given by:

$$\frac{d\sigma_{\gamma\pi}(\omega, \theta)}{d\cos\theta} = \frac{2\pi\alpha_f^2}{m_\pi^2} \cdot \left\{ F_{\gamma\pi}^{pt}(\theta) + \frac{m_\pi\omega^2}{\alpha_f} \cdot \frac{\bar{\alpha}_\pi(1 + \cos^2\theta) + 2\bar{\beta}_\pi\cos\theta}{(1 + \frac{\omega}{m_\pi}(1 - \cos\theta))^3} \right\}. \quad (5)$$

Here,  $t_0 = (m_\pi\omega/p_b)^2$ , with  $p_b$  the incident pion beam momentum in the laboratory,  $\theta$  the scattering angle of the real photon relative to the incident virtual photon direction in the alab frame,  $\omega$  the energy of the virtual photon in the alab frame,  $Z$  the nuclear charge,  $m_\pi$  the pion mass,  $\alpha_f$  the fine structure constant, and  $\bar{\alpha}_\pi$ ,  $\bar{\beta}_\pi$  the pion electric and magnetic polarizabilities. The energy of the incident virtual photon in the alab (pion rest) frame is:

$$\omega \sim (s - m_\pi^2)/2m_\pi. \quad (6)$$

The function  $F_{\gamma\pi}^{pt}(\theta)$  describing the Thomson cross section for  $\gamma$  scattering from a point pion is given by:

$$F_{\gamma\pi}^{pt}(\theta) = \frac{1}{2} \cdot \frac{1 + \cos^2\theta}{(1 + \frac{\omega}{m_\pi}(1 - \cos\theta))^2}. \quad (7)$$

From Eq. 5, the cross section depends on  $(\bar{\alpha}_\pi + \bar{\beta}_\pi)$  at small  $\theta$ , and on  $(\bar{\alpha}_\pi - \bar{\beta}_\pi)$  at large  $\theta$ . A precise fit of the theoretical cross section (Eq. 4-7) to the measured angular distribution of scattered  $\gamma$ 's, allows one to extract the pion electric and magnetic polarizabilities. Fits will be done for different regions of  $\omega$  for better understanding of the systematic uncertainties. We will carry out analyses with and without the dispersion sum rule constraint (Holstein [1990]) that  $\bar{\alpha}_\pi + \bar{\beta}_\pi \approx 0.4$ . We can achieve a significantly smaller uncertainty for the polarizability by including this constraint in the fits.

The event generator produces events in the alab frame, characterized by the kinematical variables  $t$ ,  $\omega$  and  $\cos\theta$ , and distributed with the probability, of the theoretical Compton Primakoff cross section (Eq. 4-7). Then, the  $\gamma\pi$  scattering kinematics are calculated. The virtual photon incident along the recoil direction  $\mathbf{k}/|k|$ , is scattered on the pion "target", and emerges as a real photon with energy/momentum  $\omega'/k'$  at an angle  $\theta$ :

$$\omega' = \frac{\omega(1 + \frac{\omega^2 - k^2}{2m_\pi\omega})}{1 + \frac{\omega}{m_\pi}(1 - \frac{k}{\omega}\cos\theta)} \quad (8)$$

The photon azimuthal angle around the recoil direction is randomly generated using a uniform distribution. The four-vector components of all reaction participants (pion, photon and recoil nucleus) are then calculated in the alab frame. The azimuthal angle of the recoil nucleus is also randomly generated by a uniform distribution. Finally, the reaction kinematics are transformed to the lab frame by a Lorentz boost.

For the measurement of the pion polarizabilities, one must fit the theoretical cross section (4-7) to measured distributions, after correcting for acceptances.

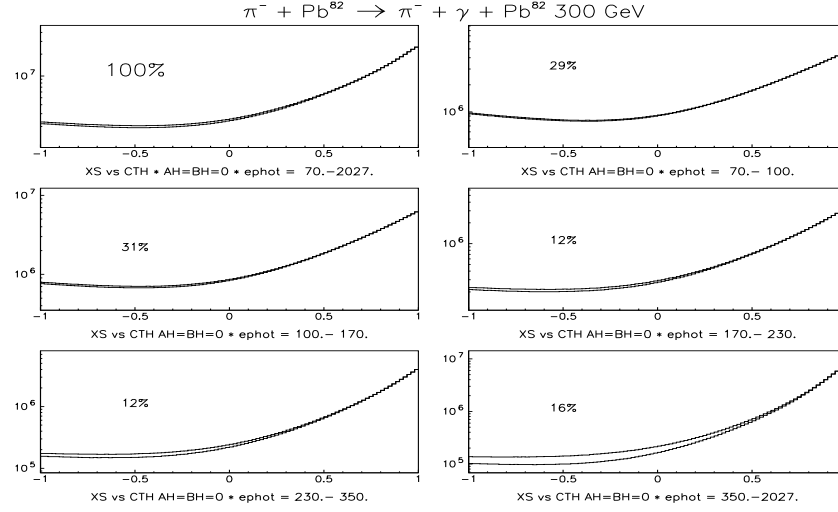


**Fig. 3.** The dependence of the theoretical angular distributions on polarizability for different regions of  $\gamma$  energy  $\omega$  (given in MeV), function of  $\cos(\theta)$  in the alab frame. The lower curve corresponds to  $\bar{\alpha}=7$ ,  $\bar{\beta}=-6$ ; while the upper curve corresponds to zero polarizabilities. The percentage shows the statistics fraction in each  $\omega$  region.

The sensitivity to the polarizability increases with increasing  $\omega$  energy and at back angles. A convenient method is to use the  $\cos\theta$  distribution integrated over  $t$  and  $\omega$ , since this shows clearly the sensitivity to the polarizability. The sensitivities of the theoretical angular distributions to the polarizabilities (i.e., for  $\bar{\alpha}=\bar{\beta}=0$  and for  $\bar{\alpha}=7$ ,  $\bar{\beta}=-6$ ) for different regions of  $\omega$  are given in Fig. 3-4. The per cent statistics for different  $\omega$  regions are shown in Fig. 3.

### 3.3 Design of the Primakoff Trigger

The small Primakoff cross section and the high statistics required for extracting polarizabilities require a data run at high beam intensities and with good acceptance. This sets the main requirements for the trigger system: (1) to act as a "beam killer" to suppress the high rate background associated with non-interacting beam pions, (2) to avoid cutting the acceptance at the important  $\gamma$  back angles in the alab frame, where the hadron polarizability measurement is most sensitive, (3) to cope with background in the  $\gamma$  calorimeter from low energy  $\gamma$ 's or delta electrons.

COMPASS plans to construct a Primakoff trigger that incorporates a veto of the non-interacting beam in a window on the hadron energy in HCAL2, and which includes a coincidence of the scattered pion with a  $\gamma$  measured in the ECAL2 calorimeter. We studied the feasibility of such a trigger, via simulations carried out at 300 GeV (Moinester et al. [1997]).



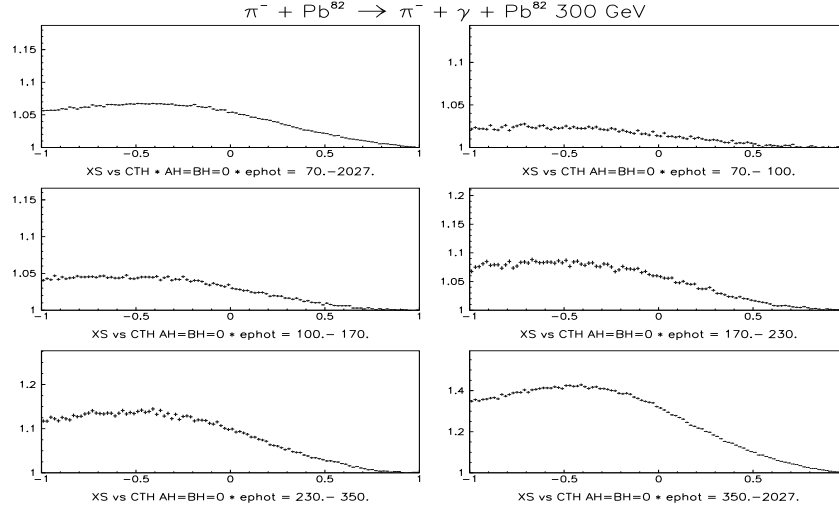


**Fig. 4.** Ratio of the theoretical angular distributions for different regions of  $\gamma$  energy  $\omega$  (given in MeV), as a function of  $\cos(\theta)$  in the alab frame, for the case of zero polarizabilities (Thomson term only), relative to the case in which  $\bar{\alpha}=7$ ,  $\bar{\beta}=-6$ . The contribution of the polarizability to the cross section is larger at back alab angles, and increases with increasing  $\omega$ .

For the reaction given in Eq. 1, the laboratory outgoing  $\gamma$ 's are emitted within an angular cone of within 5 mrad, and the corresponding outgoing  $\pi$ 's are emitted within 2 mrad. Most events have  $\gamma$  energies between 0 – 280 GeV, and  $\pi$  energies between 20 – 300 GeV. The kinematics are shown in Fig. 5. The recoil nucleus of mass  $M$  for a Primakoff reaction has negligible recoil energy ( $T_r \approx t/2M$ ), with roughly 99% of the events having recoil kinetic energies less than 30 MeV. The corresponding final state  $\pi$  and  $\gamma$  carry all the four momentum of the beam pion. Momentum and energy conservation may be used at the analysis stage for background suppression.

Our MC shows that we lose very little polarizability information by applying an "energy cut" trigger condition that rejects events with the outgoing pion energy having more than 240 GeV. Correspondingly, the final state  $\gamma$  has less than 60 GeV. The 240 GeV cut value was devised to act as a beam killer, as discussed in more detail below. The 60 GeV cut will also be very effective in reducing the  $\gamma$  detector (ECAL2) trigger rate, since a large part of the background  $\gamma$  rate is below 60 GeV.

The polarizability insensitivity to these cuts results from the fact that the most forward (in alab frame) Compton scattering angles have the lowest laboratory  $\gamma$  energies and largest laboratory angles. In addition, the cross section in this forward alab angle range is much less sensitive to the polarizabilities. This is seen from Eq. 5, since with  $\bar{\alpha}_\pi + \bar{\beta}_\pi \approx 1$  used in our MC, the polarizability

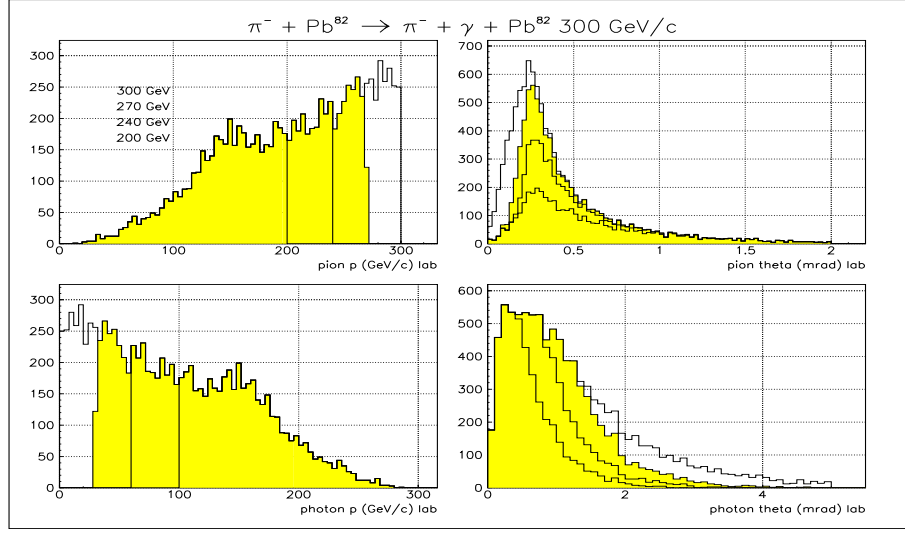


**Fig. 5.** MC simulation showing the kinematics of the  $\gamma\pi \rightarrow \gamma\pi$  reaction, in terms of the  $\pi$  and  $\gamma$  momenta and angles. The overlaid spectra correspond to different trigger cuts on the final state  $\pi$  momentum.

component is small at forward compared to back angles. The acceptance is reduced by the energy cut for the forward alab angles (shown in Fig. 6), but is unaffected at the important alab back angles. Summarizing, the pion and  $\gamma$  energy constraints at the trigger level fulfill the "beam killer" requirement and at the same time remove backgrounds coming from low energy  $\gamma$ 's, delta electrons, and  $e^+e^-$  pairs incident on ECAL2, etc.

### 3.4 Beam Requirements

In COMPASS, two beam Cherenkov detectors (CEDARS) far upstream of the target provide  $\pi/K/p$  particle identification (PID). The incoming hadron momentum is measured in the beam spectrometer. Before and after the target, charged particles are tracked by high resolution silicon strip tracking detectors. The measurement of both initial and final state momenta provides constraints to identify the reaction. The final state hadron and  $\gamma$  momenta are measured downstream in the magnetic spectrometer and in the  $\gamma$  calorimeter, respectively. These measurements allow a precise determination of the small  $p_T$  kick to the target nucleus, the main signature of the Primakoff process, and the means to separate Primakoff from diffractive scattering events.

We can get quality statistics for the pion study with high beam intensities at the CERN SPS. Some of the detectors needed for this study (such as HCAL2 modules with a signal duration of about 50 nsec) must accept the full beam intensity, and cannot tolerate beam intensities higher than 5 MHz. We will take

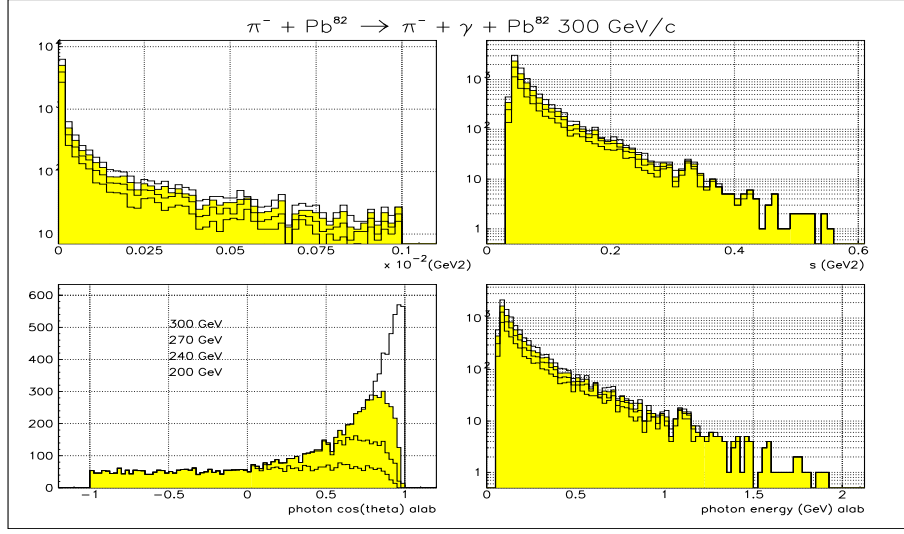


**Fig. 6.** MC simulation showing the acceptance of the  $\gamma\pi \rightarrow \gamma\pi$  reaction in terms of the invariant four momentum transfer  $t$  to the target, the squared invariant energy  $s$  of the final state  $\gamma\pi$ , the angular distribution versus  $\cos(\theta)$  with  $\theta$  the  $\gamma$  scattering angle in the alab frame, and the virtual photon energy  $\omega$  in the alab frame. The overlaid spectra correspond to different cuts on the final state  $\pi$  momentum.

data with different beam energies and targets, with both positive and negative beams, as part of efforts to control systematic errors.

### 3.5 Target and Target Detectors

The main Primakoff target will be Pb which has approximately a 1.2 mb Compton scattering (polarizability) cross section and total inelastic cross section of 1.8 barn. For a COMPASS pion beam rate of 5 MHz during the 2.5 second beam spill (every 19 seconds), and a 1% interaction Pb target, we therefore expect approximately 80 events per spill ( $80 \approx 1.2/1.8 \times 10^{-3} \times 10^{-2} \times 5. \times 10^6 \times 2.5$ ) from the pion Primakoff effect. We also need Primakoff scattering on nuclei with  $Z < 82$  to check the expected  $Z^2$  cross section dependence.

The target is followed by two scintillation interaction counters (IC) with a triggering condition of 1 minimum ionizing particle (mip) each (see Fig. 1). We use Si tracking detectors before and immediately after the targets. We veto target break-up events by selecting 1 mip in the IC counters after the targets, and by selecting low- $t$  events in the off-line analysis.

### 3.6 The Magnetic Spectrometer and the $t$ -Resolution

We need good momentum resolution for the incident and final state pions and  $\gamma$ 's. In this way, the important four momentum  $t$  resolution can be kept as good

as possible. A final state  $\pi^-$  at 200 GeV/c can be momentum analyzed to 2 GeV/c resolution, with better resolution at lower momenta.

The angular resolution for the final state  $\pi$  can be controlled by minimizing the multiple scattering in the targets and detectors. With a lead target of 1% interaction length (2 g/cm<sup>2</sup>, 30% radiation length), multiple Coulomb scattering (MCS) of the beam and outgoing pion in the target gives an rms angular resolution of order 40  $\mu$ rad. The intrinsic silicon tracking detector angular resolution is significantly better than the MCS contribution to the angular resolution. We estimate the resolution of the transverse momentum  $p_T$  by considering the  $p_T$  generated through MCS for a non-interacting straight-through beam pion of 200 GeV. The  $p_T$  given to such a beam pion (with no Compton scattering) is then  $p_T = p \times \Delta\theta = 200 \times 40 \times 10^{-6} = 8$  MeV, which corresponds to  $t = p_T^2 = 0.6 \times 10^{-4} \text{ GeV}^2$ . This sets the inherent uncertainty  $\Delta t$  in determining  $t = p_T^2$  for Compton scattering events.

We aim to achieve  $\Delta t$  of order  $\approx 10^{-4} \text{ GeV}^2$  over the energy range 40-240 GeV, in order to allow an effective  $t$ -cut to minimize contributions to the data from the strong processes that occur at large  $t$ . This goal is based on the  $t$  distributions measured at a 200 GeV low statistics, high resolution experiment for  $\pi^- \rightarrow \pi^- \pi^0$  (Jensen et al. [1983]) and  $\pi^- \rightarrow \pi^- \gamma$  (Zielinski et al. [1984]) Primakoff scattering at 200 GeV at FNAL. The  $t$  distribution of the  $\pi^- \rightarrow \pi^- \gamma$  data agrees well with the Primakoff formalism out to  $t = 10^{-3} \text{ GeV}^2$ , which indicates that the data are indeed dominated by Coulomb production. Minimum material (radiation and interaction lengths) in COMPASS will also give a higher acceptance, since that allows  $\gamma$ 's to arrive at ECAL2 with minimum interaction losses, and minimum  $e^+e^-$  backgrounds.

### 3.7 The $\gamma$ Calorimeter ECAL2

COMPASS will be able to measure a final state 200 GeV  $\gamma$  to  $\pm 2$  GeV, with a position resolution of 1.5 mm, in the second  $\gamma$  calorimeter ECAL2. This  $\gamma$  detector is equipped with 3.8 by 3.8 cm<sup>2</sup> GAMS lead glass blocks to make a total active area of order 1.5 m diameter. An exotic hybrid meson study ( $\pi\eta$  detection) that will run simultaneously with the polarizability/anomaly study fixes the area of ECAL2 (Moinester et al. [1997]). The area needed for the polarizability measurement is only 30 $\times$ 30 cm<sup>2</sup>.

The  $p_T$  kicks of the two COMPASS magnets are 0.45 GeV/c for SM1 (located 4 meters downstream of the target) and 1.2 GeV/c for SM2 (16 meters from target). We require the highest conveniently accessible effective  $p_T$  kick for this physics. The fields of both magnets must therefore be set *additive* for maximum deflection of the beam from the zero degree (neutral ray) line. ECAL2 should be at maximum distance from the target ( $\approx 40$  meters) to also maximize the distance between the zero degree line and the deflected non-interacting beam position. ECAL2 has a hole through which the beam passes and hits HCAL2.

We need to attain at least 10 cm for the distance between the zero degree line and the hole edge. This is so since the Primakoff  $\gamma$ 's are concentrated around the

zero degree line and a good  $\gamma$  measurement requires clean signals from 9 blocks, centered on the hit block. The beam hole size and position must be optimized to minimize the hadrons hitting ECAL2 blocks at the hole perimeter. We plan it to be big enough (2 blocks V  $\times$  16 blocks H) to pass completely the non-interacting beam, and to pass also the majority of Primakoff scattered pions. In that way, these particles are measured well in the HCAL2 hadron calorimeter behind ECAL2. We are then able to optimally fix the beam killer threshold cut.

From MC simulations, the number of Primakoff scattered pions below 40 GeV is less than 0.3%, so that 40 GeV pions are about the lowest energy of interest. We will effectively set a  $\pi^-$  acceptance energy window of 40 - 240 GeV, via a minimum threshold of 60 GeV for the  $\gamma$  energy deposited in ECAL2, and an HCAL2 veto for energies above 240 GeV.

### 3.8 The Hadron Calorimeter HCAL2

We intend to use beam rates of order 5 MHz, where the rate limit is the maximum allowed for good operation of the existing and tested  $15 \times 15 \text{ cm}^2$  Dubna hadron calorimeter modules. For the beam killer trigger purposes, we require a mini-HCAL2 configured as an array of  $15 \times 15 \text{ cm}^2$  blocks ( $2 \times 2$  or  $3 \times 3$ ) to catch non-interacting beam pions. As shown in Fig. 1, we will actually use a larger HCAL2. But the energy sum for trigger purposes would still be taken from the mini-HCAL2. The HCAL2 modules have energy resolution of  $\pm 15 \text{ GeV}$  at 300 GeV. Together with the beam acceptance of  $\pm 13 \text{ GeV}$ , we can achieve a  $1\text{-}\sigma$  identification of the beam via a detection window of  $300 \pm 20 \text{ GeV}$ . We can therefore set a  $3\text{-}\sigma$  discriminator veto threshold at  $300 - 3 \times 20 = 240 \text{ GeV}$ , to veto 99% of the beam. We will reduce the beam acceptance to 13 GeV rms or lower, by collimation. In Table 1, we estimate the ECAL2/HCAL2 effect on the Primakoff trigger. The mini-HCAL2 modules analog signals will be electronically summed and discriminated to provide a veto trigger signal for hadron energies above 240 GeV.

### 3.9 The Primakoff Trigger

We design the Primakoff trigger using three trigger levels. The final trigger signals should be developed in the minimum time possible (to reduce dead time), and within the 300-1000 nsec allowed in the COMPASS data acquisition. The T0 trigger is a fast logic signal defining the beam phase space, rate and purity at the target, and is generated near the target about 20 nsec after beam passage. It is produced via a logic relation between signals from an ensemble of beam transmission and beam halo veto (hole) scintillators located before the target. The T1 trigger exploits the essential feature of a Primakoff polarizability (and chiral anomaly) event; namely, a coincidence between a  $\gamma$  in ECAL2 and a scattered Primakoff pion. The detectors are shown in Fig. 1.

The IC counter logical signal should correspond to an amplitude of one 1 mip. BP (Beam or Primakoff) is a scintillator fiducial trigger scintillation detector

with dimensions of order 60 cm (in H) by 15 cm (in V), which is the size covered by the non-interacting pion beam and the Primakoff scattered pions. BP helps form the pion detection trigger; it is set to fire on a 1 mip window condition. The vertical size of this BP detector is larger than the 10 cm needed for polarizability. This is so in order to catch also the scattered  $\pi^-$ 's associated with the  $\pi^-\pi^0$  and  $\pi^-\eta$  final states from the chiral anomaly and hybrid meson triggers, since there is a larger angular spread of the  $\pi^-$ 's from these channels (Moinester et al. [1997]).

CP is a charged particle veto scintillator array positioned at the front face of ECAL2. It is designed with a hole slightly larger than the BP detector, in which the BP detector above is positioned. It covers the front face of ECAL2. CP protects ECAL2 from charged particles. Simulations in progress will help fix the definitive sizes of BP, CP, and the ECAL2 beam hole.

The first level trigger T1 is defined as:

$$T1 = IC(1 \text{ mip}) \cdot BP(1 \text{ mip}) \cdot \overline{CP} \cdot ECAL2(> 60\text{GeV}) \cdot \overline{HCAL2}(> 240\text{GeV}). \quad (9)$$

The trigger is designed to accept only events in which one Primakoff scattered pion hits and fires IC and BP, the  $\gamma$  energy exceeds 60 GeV, and HCAL2 does not measure more than 240 GeV. All of the non-interacting  $\pi$  beam and most of the Primakoff scattered  $\pi$ 's pass through the ECAL2 hole. These pions proceed to HCAL2, where their energy is measured well. The ECAL2 low energy threshold is important to suppress low energy backgrounds.

The task of T1 is to provide a fast gate signal to start digitization (for example in the ADC-system of the calorimeter) about  $\sim 300$  ns after the beam traverses the target (see Table 1). A second level trigger T2 can be constructed if a faster T1 or more rate reduction is needed. A faster T1 is possible if the IC counter 1 mip trigger signal, which arrives the latest at the coincidence module near ECAL2, will be transferred from T1 to T2. Further rate reduction may be gained using additional trigger conditions at the T2 level. Details have been given elsewhere (Moinester et al. [1997]).

### 3.10 Expected Trigger Rates

The ECAL2  $\gamma$  signal above 60 GeV with  $\overline{HCAL2}(> 240 \text{ GeV})$  and in coincidence with BP should reduce the trigger rate from the beam rate by an estimated factor of 1000. The CP detector requirement should give at least another factor of 5 rate reduction. In this way, one may expect to achieve a trigger rate lower than the beam rate by a factor of 5000 (Moinester et al. [1997]). The rate of this signal ( $2.5 \times 10^3$  per spill in Table 1) will be significantly lower than the maximum of  $10^5$  per spill trigger rate planned for the COMPASS data acquisition.

We need to study more precisely the background rates, and ways to reduce backgrounds. For this purpose, we will use an event generator for pion-nucleus interactions, embedded in the COMPASS apparatus. We will study what fraction of the events generated pass our trigger conditions. The factor 1000 reduction

Signature	Amp. range	Timing (nsec)	Reduc. fact.	Rate (events/spill)
Beam	—	0	—	$1.25 \cdot 10^7$
IC (interaction counter)	1 mip	1	—	$1.25 \cdot 10^7$
BP (beam or Primakoff)	1 mip	200	—	$1.25 \cdot 10^7$
CP (charged particles)	$\geq 1$ mip	200	5	$2.5 \cdot 10^6$
HCAL2 ( $\pi$ energy)	$< 240$ GeV	260	—	—
ECAL2 ( $\gamma$ energy)	$> 60$ GeV	260	1000	$2.5 \cdot 10^3$
			—	—

**Table 1.** The Primakoff trigger conditions and estimation of timing relative to the target crossing time, and trigger rate reduction. For HCAL2 and ECAL2, we consider coincidences and a common reduction factor.

above is only a guess of what we expect from the  $\gamma\pi$  coincidence condition. The trigger conditions are summarized in Table 1.

### 3.11 Measurement Significance

The experimental pion polarizability determination to date has large uncertainties; and kaon polarizabilities have never been measured. We will determine the  $\gamma\pi$  and  $\gamma K$  Compton cross section in the lab frame versus  $\omega$  and  $\cos(\theta)$ . We consider now the uncertainties achievable for the pion polarizabilities in the COMPASS experiment, based on Monte Carlo simulations.

We estimated 80 events/spill from the pion Primakoff effect (see Sec. 3.5), corresponding to  $10^7$  events per month at 100% efficiency. We assume a trigger efficiency of 50% (due to the energy cuts), an accelerator operating efficiency of 50%, and a tracking efficiency of 80%. One may then expect to observe as many as  $2 \times 10^6$  Primakoff Compton events per month of operation, following setup of COMPASS. Statistics of this order will allow systematic studies, with fits carried out for different regions of  $\omega$ ,  $Z^2$ , etc.; and polarizability determinations with statistical uncertainties of order 0.2. For the kaon polarizability, due to the lower beam intensity, the statistics will be roughly 50 times lower. A precision kaon polarizability measurement requires more data taking time.

Comparing chiral anomaly to polarizability data, we expect roughly 300 times lower statistics, due to the 140 times lower cross section and the lower  $\pi^0$  detection efficiency (Moinester [1995]).

## 4 Conclusions

The beams at CERN invite hadron Compton scattering and radiative transition studies for different particle types, such as  $\pi^{+,-}$ ,  $K^{+,-}$ ,  $p$ ,  $\bar{p}$ , and others. COMPASS will measure the  $\gamma\pi$  and  $\gamma K$  Compton scattering cross sections,

thereby enabling determinations of the pion and Kaon polarizabilities. COMPASS will also measure the formation and decay of the  $a_1(1260)$  and other resonances, and also the chiral anomaly amplitude  $F_{3\pi}$ . The pion and Kaon experiments will allow serious tests of  $\chi$ PT; and of different available polarizability and radiative decay calculations in QCD. We also described FNAL SELEX E781 attempts to study related physics via the interaction of 600 GeV pions with target electrons.

## 5 Acknowledgments

This research was supported by the U.S.-Israel Binational Science Foundation (BSF) and the Israel Science Foundation founded by the Israel Academy of Sciences and Humanities, Jerusalem, Israel. Special thanks are due to the M.P.I. Heidelberg SELEX/COMPASS group, U. Dersch, F. Dropmann, I. Eschrich, H. Kruger, J. Pochodzalla, B. Povh, J. Simon, and K. Vorwalter, for hospitality and collaboration during the writing of this report. Thanks are due to M. Buenerd, D. Drechsel, T. Ferbel, A. Ocheraschvili, S. Paul, J. Russ, I. Savin, H.-W. Siebert, A. Singovsky, and T. Walcher for valuable discussions.

## References

- F. Bradamante, S. Paul et al., CERN Proposal COMPASS, CERN/SPSLC 96-14, SPSC/P 297, <http://wwwcompass.cern.ch/>
- M. A. Moinester, in Proc. Workshop on Chiral Dynamics, M.I.T., July 1994, Eds. A. Bernstein and B. Holstein, Springer-Verlag, 1995, HEP-PH/9409463.
- B. R. Holstein, *Comments Nucl. Part. Phys.* **19**, 239 (1990).
- D. Babusci, S. Bellucci, G. Giordano, G. Matone, A. M. Sandorfi, M. A. Moinester, *Phys. Lett. B* **277**, 158 (1992).
- Yu. M. Antipov et al., *Phys. Lett. B* **121**, 445 (1983), *Z. Phys. C* **26**, 495 (1985).
- T. Jensen et al., *Phys. Rev. D* **27**, 26 (1983).
- M. Zielinski et al., *Phys. Rev. Lett.* **52**, 1195 (1984).
- A. S. Galperin et al., *Sov. Jour. Nucl. Phys.* **32**, 545 (1980).
- L. Xiong, E. Shuryak, G. Brown, *Phys. Rev. D* **46**, 3798 (1992).
- D. Ebert, M. K. Volkov, *Phys. Atom. Nucl.* **60**, **796**, (1997).
- R. Edelstein et al., Fermilab proposal SELEX E781, <http://fn781a.fnal.gov/>; J. Russ, *Nucl. Phys. A* **585**, 39 (1995).
- D. Drechsel et al, PRC **55**, 424 (1997); and private communication.
- P. A. M. Guichon et al., *Nucl. Phys. A* **591**, 606 (1995).
- M. Zielinski et al., *Phys. Rev. D* **29**, 2633 (1984).
- B. R. Holstein, *Phys. Rev. D* **53**, 53,4099 (1996).
- M. A. Moinester, in "Physics with GeV-Particle Beams", Eds. H. Machner and K. Sistemich, World Scientific, 1995, HEP-PH/9409307.
- J. Gasser and H. Leutwyler, *Nucl. Phys. B* **250**, 465 (1985).
- V. Steiner, M. A. Moinester, M. Buenerd, POLARIS, A Monte Carlo event generator for polarizability experiments. V. Steiner, M. A. Moinester, ANOMALY, A Monte Carlo event generator for chiral anomaly experiments, 1995 (unpublished).



N. I. Starkov et al., *Sov. Jour. Nucl. Phys.* **36**, 1212 (1982).

M. A. Moinester et al., COMPASS Report, 1997, <http://vsnhd1.cern.ch/~murraym>